

# Verifying ASCE 41 the evaluation model via field tests of masonry infilled RC frames with openings

Chun-Ting Huang<sup>1a</sup>, Tsung-Chih Chiou<sup>\*2b</sup>, Lap-Loi Chung<sup>1,2c</sup>, Shyh-Jiann Hwang<sup>1,2c</sup> and Wen-Ching Jaung<sup>3b</sup>

<sup>1</sup>Department of Civil Engineering, National Taiwan University, Taipei, Taiwan

<sup>2</sup>National Center for Research on Earthquake Engineering, NARLabs, Taipei, Taiwan

<sup>3</sup>Jaung Wen-Ching Civil Engineering Office, Hualien, Taiwan

(Received January 30, 2020, Revised July 9, 2020, Accepted August 20, 2020)

**Abstract.** The in-situ pushover test differs from the shake-table test because it is performed outdoors and thus its size is not restricted by space, which allows us to test a full-size building. However, to build a new full-size building for the test is not economical, consequently scholars around the world usually make scale structures or full-scale component units to be tested in the laboratory. However, if in-situ pushover tests can be performed on full-size structures, then the seismic behaviors of buildings during earthquakes can be grasped. In view of this, this study conducts two in-situ pushover tests of reinforced concrete (RC) buildings. One is a masonry-infilled RC building with openings (the openings ratio of masonry infill wall is between 24% and 51%) and the other is an RC building without masonry infill. These two in-situ pushover tests adopt obsolescent RC buildings, which will be demolished, to conduct experiment and successfully obtain seismic capacity curves of the buildings. The test results are available for the development or verification of a seismic evaluation model.

This paper uses ASCE 41-17 as the main evaluation model and is accompanied by a simplified pushover analysis, which can predict the seismic capacity curves of low-rise buildings in Taiwan. The predicted maximum base shear values for masonry-infilled RC buildings with openings and for RC buildings without masonry infill are, respectively, 69.69% and 87.33% of the test values. The predicted initial stiffness values are 41.04% and 100.49% of the test values, respectively. It can be seen that the ASCE 41-17 evaluation model is reasonable for the RC building without masonry infill walls. In contrast, the analysis result for the masonry infilled RC building with openings is more conservative than the test value because the ASCE 41-17 evaluation model is limited to masonry infill walls with an openings ratio not exceeding 40%. This study suggests using ASCE 41-17's unreinforced masonry wall evaluation model to simulate a masonry infill wall with an openings ratio greater than 40%. After correction, the predicted maximum base shear values of the masonry infilled RC building with openings is 82.60% of the test values and the predicted initial stiffness value is 67.13% of the test value. Therefore, the proposed method in this study can predict the seismic behavior of a masonry infilled RC frame with large openings.

**Keywords:** masonry infill; openings; in-situ pushover test; reinforced concrete; ASCE 41

## 1. Introduction

Given that in-situ pushover tests are performed outdoors, the size of the test is not limited by the location. Consequently, a full-size building can be used, which is the most direct way to capture the behavior of a structure. However, to build a new full-size building for testing is not economical, consequently scholars around the world usually make scale structures or full-scale structural components for testing in the laboratory. Currently, reinforced concrete (RC) buildings are the most common structures. However, owing to the need for lighting, ventilation, and accessibility for this type of building, it is necessary to construct a brick wall on the column side to assist the door and window configuration. Consequently, RC buildings with masonry

infill and openings are formed.

During earthquakes, masonry infill walls with openings can provide lateral force and initial in-plane stiffness for the frames. However, the columns are easily damaged by brick walls and the columns cannot achieve their full potential seismic capacity. A photo of an example of this sort of damage is shown in Fig. 1.

If engineers conducting analysis ignore the existence of masonry infill walls with openings, then it is easy to underestimate the lateral force and overestimate the toughness of RC buildings. To understand the seismic behavior of RC buildings with masonry infill and openings, many studies have conducted tests on scaled-down in size RC frames with masonry infill and openings in the laboratory. These tests relate to single-span single-story buildings (Kakaletsis and Karayannis 2007, Kakaletsis and Karayannis 2008, Asteris *et al.* 2011, Sigmund and Penava 2012, Mansouri *et al.* 2013, Bergami and Nuti 2015, Okail *et al.* 2016, Tekeli and Aydin 2017, Wang *et al.* 2019, Maidiawati *et al.* 2019, Ahani *et al.* 2019, Penava *et al.* 2019), or multi-span multi-story buildings (Mosalam *et al.* 1997, Al-Chaar *et al.* 2003, Voon and Ingham 2008,

\*Corresponding author, Ph.D.

E-mail: [tcchiou@narlabs.org.tw](mailto:tcchiou@narlabs.org.tw)

<sup>a</sup>Ph.D. Candidate

<sup>b</sup>Ph.D.

<sup>c</sup>Ph.D. Professor



Fig. 1 Photographs of columns that are damaged by infill wall segments

Stavridis *et al.* 2012, Balik *et al.* 2013, Fenerci *et al.* 2016, Lourenço *et al.* 2016, Ozturkoglu *et al.* 2017, Shah *et al.* 2019, Aknouche *et al.* 2019). Because of the spacing limitation of the laboratory, specimen size is limited to partial components or scaled-down structures. Therefore, a full-size masonry infilled RC frame with openings in-situ pushover test is essential.

In view of the lack of data from in-situ pushover tests of full-size RC buildings with masonry infill and openings, the National Center for Research on Earthquake Engineering in Taiwan (hereinafter abbreviated as NCREE) used an obsolete low-rise school building for an in-situ monotonic pushover test to understand the seismic behavior of a masonry infilled RC frame with openings during earthquakes. The in-situ pushover tests of RC building conducted in this study were carried out by NCREE (Jiang *et al.* 2008). These RC school buildings were located in Yunlin, Taiwan. It was built in 1956 and were due to be demolished. However, before the RC school building were demolished, NCREE divided the RC school building into three test units: a pure RC frame without masonry infill, a masonry infilled RC frame with openings, and an RC frame retrofitted with wing-wall. This study focuses on the seismic behavior of the first two buildings and it compares the results with the behavior of RC buildings with or without masonry infill. Therefore, we will only cover the test plan, size of tests, force system, material parameters, and experimental observations of the RC school building for the first two in-situ pushover tests.

This study uses ASCE/SEI 41-17 (ASCE 2017) as the main evaluation model, which was revised in 2017 and verified shake-table tests of a 2-span, three-story planar RC frame (Stavridis *et al.* 2012). There are two spans of planar RC frames per floor, one of which contains a masonry-infilled wall and the other span contains a masonry-infilled wall with an opening. The masonry-infilled wall with one opening with an area equal to the total masonry-infilled wall area has an openings ratio of less than 40%, which is just applicable for the ASCE/SEI 41-17 (ASCE 2017) evaluation model. However, the test is only of a planar RC frame and it cannot fully represent a real RC building. In addition, the openings ratio of the masonry-infilled wall with one opening is often greater than 40%, which cannot be applied to the ASCE/SEI 41-17 (ASCE 2017) evaluation model. The RC buildings with masonry infill and openings used in the in-situ pushover tests in this study have

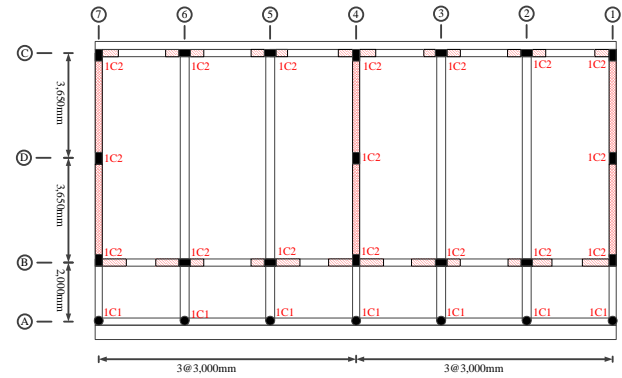


Fig. 2 Plan of the first floor of specimen MI

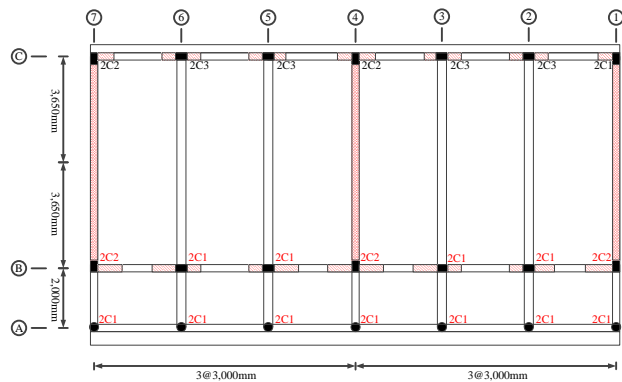


Fig. 3 Plan of the second floor of specimen MI

openings ratios for the masonry infill walls of between 24% and 51%, which can be used to verify the scope of application of the ASCE/SEI 41-17 (ASCE 2017) evaluation model. This paper will cover the in-situ pushover test of the RC school buildings and the evaluation model of ASCE/SEI 41-17 (ASCE 2017). It will also analyze and discuss the prediction results.

## 2 School building field experiments

### 2.1 Experimental plan

A large number of school buildings were damaged in the 1999 Chi-Chi Earthquake in Taiwan. However, the damage was concentrated on vertical members such as columns and masonry infill walls with openings along corridors. The floor slabs and beams were connected together, so the stiffness of the beams was stronger than the design demands, and consequently the beams were damaged slightly or were undamaged. The collapsed RC school buildings were damaged in a weak-column strong-beam mode. The vertical members along the corridors of RC school buildings played the main role in resisting the earthquake. Therefore, to understand the seismic behaviors of school buildings subjected to lateral force, the lateral force loading system for this in-situ monotonic pushover test was set along the corridor direction for the experiment.

This study conducts two test units in-situ pushover tests of RC school buildings. This test units are two-story. The

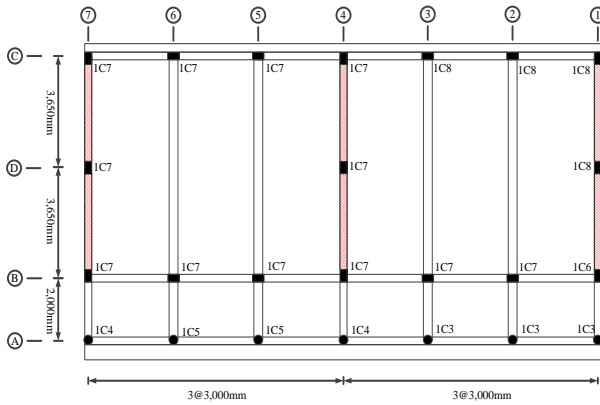


Fig. 4 Plan of the first floor of specimen BF

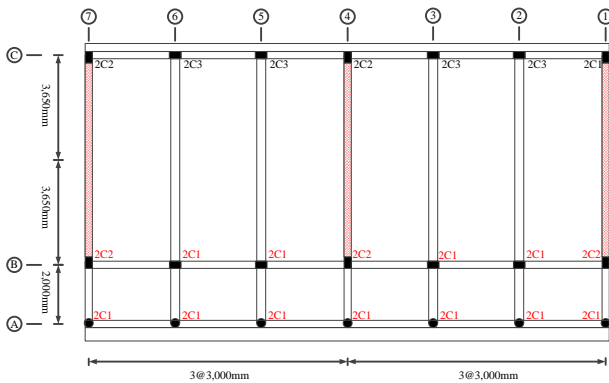


Fig. 5 Plan of the second floor of specimen BF

RC school building have eight classrooms on each floor. Two classrooms on each level are chosen as a test unit. Therefore, the RC school buildings can be divided into three test units, which are a masonry infilled RC building with openings (hereinafter referred to as an “specimen MI”), an RC building without masonry infill (hereinafter referred to as an “specimen BF”), and an RC building retrofitted by RC wing walls. To explore the differences between specimen MI and specimen BF, the first two tests will be described in the following subsection.

2.2 Test units

Specimen MI and specimen BF are both two-story test units. There are two classrooms on each floor and there are three spans in each classroom. Each span is 3,000 mm. The length of the test unit along the corridor is 18,000 mm, the length perpendicular to the corridor is 9,300 mm. Plan views of the second floor and roof floor of specimen MI and specimen BF are shown in Fig. 2 to Fig. 5, respectively.

In Fig. 2, 1C1 and 1C2 are the column cross-sections of the first floor of specimen MI. In Fig. 3, 2C1 to 2C3 are the column cross-sections of the second floor of specimen MI. In Fig. 4, 1C3 to 1C8 are the column cross-sections of the first floor of specimen BF. In Fig. 5, 2C1 to 2C3 are the column cross-sections of the second floor of specimen BF.

Frame A in specimen MI and specimen BF is the corridor column frame. The front elevation views of Frame A of specimen MI and specimen BF are shown in Fig. 6.

Frame B and Frame C in specimen MI and in specimen

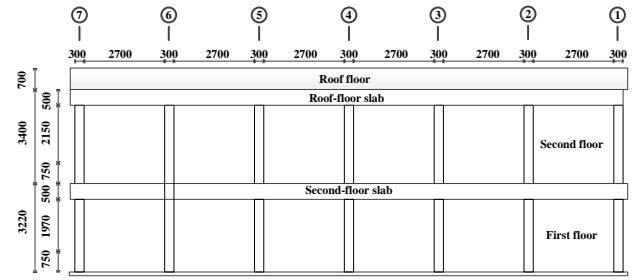


Fig. 6 Elevation view of Frame A of specimen MI and specimen BF(mm)

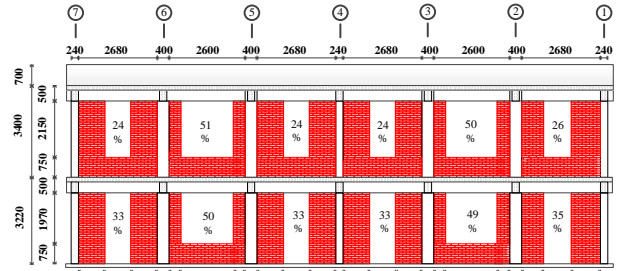


Fig. 7 Elevation view of Frame B of specimen MI(mm)

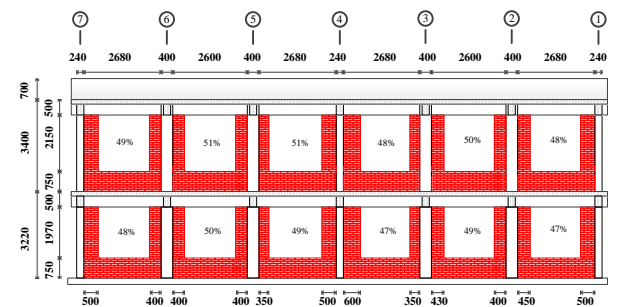


Fig. 8 Elevation view of Frame C of specimen MI (mm)

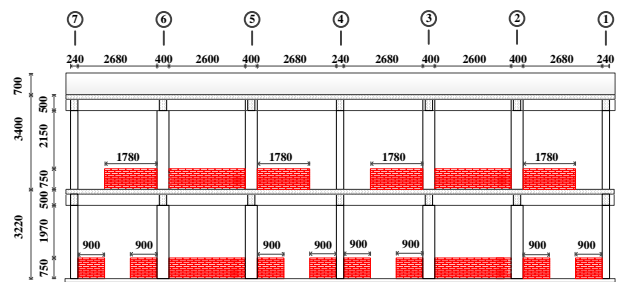


Fig. 9 Elevation view of Frame B of specimen BF (mm)

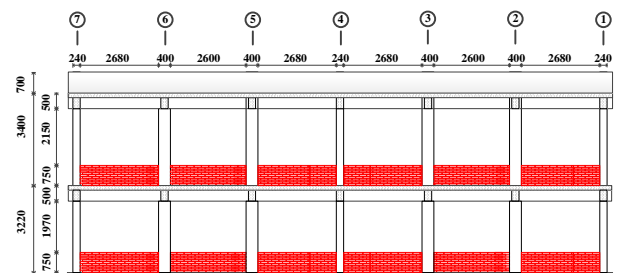


Fig. 10 Elevation view of Frame C of specimen BF(mm)

BF are the classroom column frames. The front elevation views of Frame B and Frame C of specimen MI and specimen BF are shown in Fig. 7 to Fig. 10.

Table 1 Details of test column cross-sections for school building field testing (dimensions in mm)

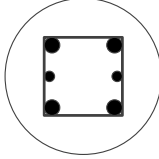
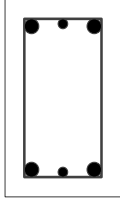
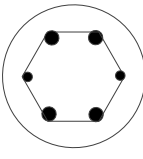
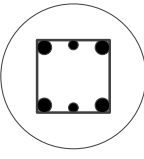
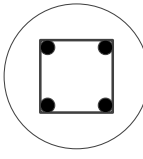
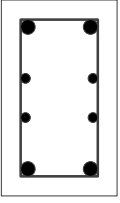
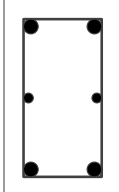
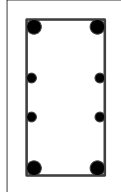
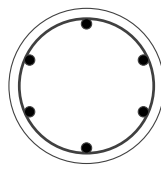
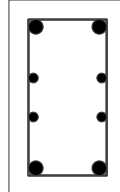
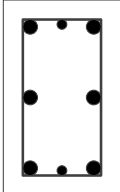
Column number	1C1	1C2	1C3	1C4	1C5	1C6
Sectional view						
Longitudinal reinforcement	● 4-R18 ● 2-R15	● 4-R18 ● 2-R15	● 4-D19 ● 2-D16	● 4-D19 ● 2-D16	4-D19	● 4-D19 ● 4-D16
Transverse reinforcement	R6@200	R6@200	D10@250	R6.4@250	R6.4@250	D10@200
Size	D300	240 × 400	D300	D300	D300	240 × 400

Table 2 Details of test column cross-sections for school building field testing (dimensions in mm)

Column number	1C7	1C8	2C1	2C2	2C3
Sectional view					
Longitudinal reinforcement	● 4-D19 ● 2-D16	● 4-D19 ● 4-D16	6-D16	● 4-D19 ● 4-D16	● 6-D19 ● 2-D16
Transverse reinforcement	R6.4@250	D10@250	D10@250	D10@250	D10@250
Size	240 × 400	240 × 400	D300	240 × 400	240 × 400

In Fig. 6 to Fig. 10, the first story height is 3,220 mm and the second story height is 3,400 mm. The windowsill height is 750 mm. Therefore, the effective length of the columns restrained by the windowsill is the height from windowsill to beam bottom.

To make the sizes of the brick walls of the first and second floors of specimen MI consistent in dimensions, the brick walls of Frames B and C are rebuilt so that the widths of the brick walls in the two levels are the same.

In Figs. 7 and 8, the openings ratio of masonry infill is  $R_{op} = \frac{A_{op}}{A_{inf}}$ , where  $A_{op}$  is the opening area of masonry infill and  $A_{inf}$  is the total area of masonry infill wall including openings.

In Fig. 7, the openings ratios of the masonry infill in each span of Frame B on the first and second floor are between 24% and 51%. In Fig. 8, the openings ratios of masonry infill in each span of Frame C on the first and second floor are between 48% and 51%. Frame D is a partition column frame, where only the first floor has partition columns.

The column cross-section of Frame A of specimen MI and specimen BF are both circular sections, both with diameters of 300 mm. The columns in the first and second floors of Frames B, C, and D are all rectangular sections, with dimensions of 240 mm × 400 mm. The column cross-sections configuration direction of specimen MI and specimen BF are shown in Fig. 2 to Fig. 5. It should be noted that the cross-sectional dimensions of the columns of

each frame in the test unit have the same sizes but the details of the rebars are different.

For the 1C1 to 1C8 column cross-section, the rebar details are shown in Tables 1 and 2. It should be noted that R18, R15, R6.4 and R6 are plain bars of 18 mm, 15 mm, 6.4 mm and 6 mm in diameter in Table 1. D19, D16 and D10 are deformed bars of 19 mm, 16 mm and 10 mm in diameter, as shown in Tables 1 and 2. The brick walls are laid by solid brick, the dimension of brick unit is 240mm long, 120 mm wide, and 60 mm thick. The thickness of the brick wall is double the width of the solid brick (i.e., 240 mm).

### 2.3 Test setup

After the Chi-Chi earthquake, many school buildings had damage concentrated in the vertical members, such as columns and masonry infill walls with openings. Therefore, the lateral force loading system for the in-situ monotonic pushover tests in this study was set along the corridor direction and the force was applied in only a single direction. A plan view for the in-situ monotonic pushover tests is given in Fig. 11.

A front elevation view for the in-situ monotonic pushover tests using specimen MI's Frame B is shown in Figure 12 for demonstration. In Figs. 11 and 12, the left-hand classrooms are the test unit, while the right-hand classrooms are the reaction unit. The black arrow is the direction of force. To install the force loading system in this

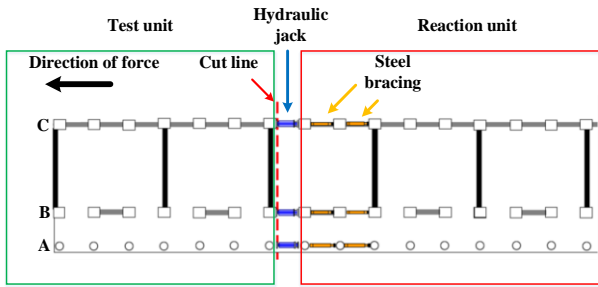


Fig. 11 Plan view of planning for field experiment (NCREE)

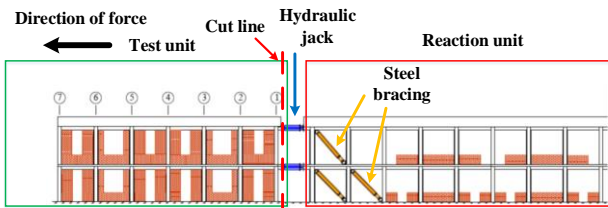


Fig. 12 Elevation view of planning for field experiment (NCREE)

experiment, the floor slab and beam were cut between the test unit and the reaction unit, and hydraulic jacks to apply force were installed on the ends of the beams on the second-floor and roof-floor of frames A, B and C, thus there were six hydraulic jacks.

The locations of the hydraulic jacks are shown in Figs. 11 and 12 at the horizontal line between the test unit and the reaction unit. The hydraulic jacks on the roof-floor and the second-floor have a piston cross-sectional area ratio of 2:1. When the same oil pressure is applied, it can provide a lateral force of 2:1, to simulate the distribution of inverted-triangular lateral force on the test unit. The value of the base shear strength obtained in the field test is the sum of the six hydraulic-jack load readings on the second-floor and the roof-floor.

In addition to acting as a supportive counterforce in the adjacent test unit classrooms, the first floor and second floor of reaction unit classrooms had steel bracing installed. The location of the steel bracing is indicated by the horizontal line spanning between frames A, B, and C of the reaction unit classrooms, as shown in Fig. 11.

The in-situ pushover tests use displacement control, which uses the reserved classroom in the test unit's free-end space as a reference frame for the displacement meter to measure the absolute displacement values of the second-floor and roof-floor in frames A, B and C. The displacement of the roof-floor is the average of the roof-floor displacement readings in frames A, B and C. The displacement meter uses the elevation of specimen MI's Frame B for demonstration, as shown in Fig. 13.

In relation to the axial load system, to simulate the weight of a four-story building, both of these tests have water tanks installed on the second floor and added unwanted soil on the roof floor. The weight of the filled water is 785kN and the weights of the unwanted soil is 1177kN. The total additional axial loads are 1962kN. The axial load system's loading diagram is shown in Fig. 14.

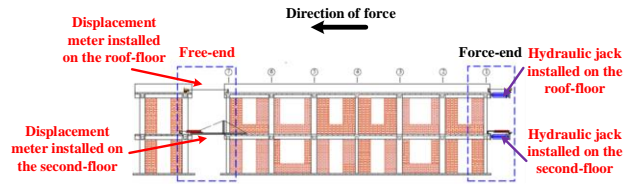


Fig. 13 Diagram of layout of displacement meters for field experiment (NCREE)

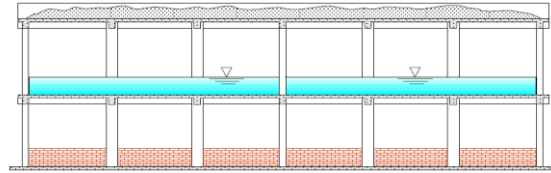


Fig. 14 Axial force loading diagram for field tests (NCREE)

Table 3 Material parameters of the columns on the school buildings' first floors

Specimen MI (MPa)	$f'_c$	$f_{yl}$ (R18)	$f_{yl}$ (R15)	$f_{yt}$ (D10)	$f_{yt}$ (R6.4)	$f'_m$	$f_{mc}$
	27.6	304	277	-	347	7	21.97
Specimen BF (MPa)	$f'_c$	$f_{yl}$ (D19)	$f_{yl}$ (D16)	$f_{yt}$ (D10)	$f_{yt}$ (R6.4)	$f'_m$	$f_{mc}$
	29.7	290	314	371	347	7	21.97

Table 4 Material parameters of the columns on the school buildings' second floors

Specimen MI (MPa)	$f'_c$	$f_{yl}$ (D19)	$f_{yl}$ (D16)	$f_{yt}$ (D10)	$f'_m$	$f_{mc}$
	27.6	280	314	371	7	30.02
Specimen BF (MPa)	$f'_c$	$f_{yl}$ (D19)	$f_{yl}$ (D16)	$f_{yt}$ (D10)	$f'_m$	$f_{mc}$
	29.7	280	314	371	7	30.02

After the test, sampling of the concrete, reinforcement, and brick is performed for subsequent material tests.

## 2.4 Field test of material strength

The first and second floor of brick infilled and specimen BF's material parameters are shown in Tables 3 and 4. In these tables,  $f'_c$  is the compressive strength of the concrete;  $f_{yl}$  is the yield strengths of longitudinal reinforcements;  $f_{yt}$  is the yield strength of transverse reinforcement;  $f'_m$  is the compressive strength of brick blocks;  $f_{mc}$  is the compressive strength of the mortar.

## 2.5 Test results

Pictures of specimen MI and specimen BF after in-situ pushover tests are shown in Fig. 15. It can be seen from Fig. 15 that after the test unit collapsed, the damage to the school building is concentrated in the vertical members of the first floor along the corridor direction.

The columns in the second floor have no obvious cracking, and elastic deformation is maintained. Therefore, the collapsed RC school buildings are damaged in a weak-



Fig. 15 Pictures of specimen MI (left-hand panel) and specimen BF (right-hand panel) after the field tests

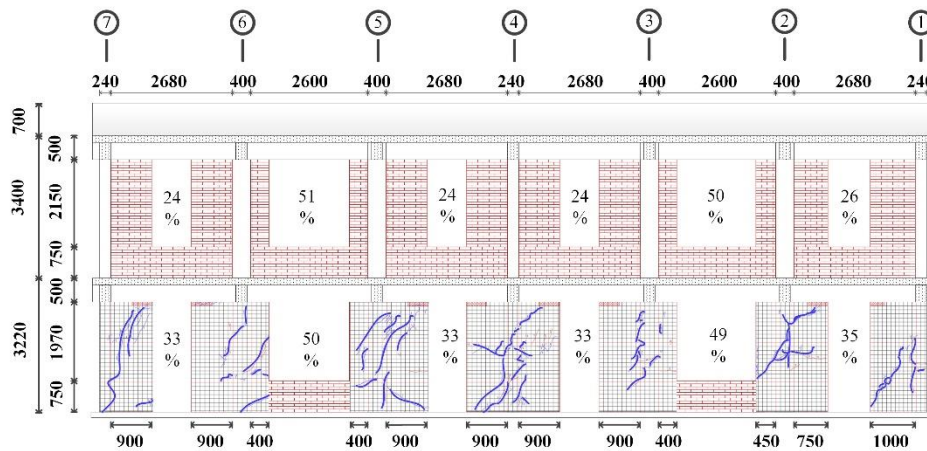


Fig. 16 Crack development of specimen MI's Frame B

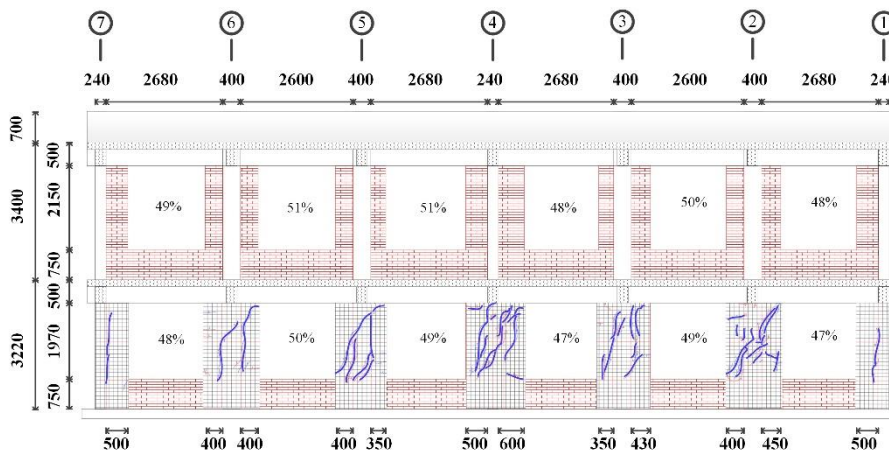


Fig. 17 Crack development of specimen MI's Frame C

column strong-beam mode. These results are the same as the damage that was observed after the Chi-Chi earthquake. Moreover, observations of the failure modes and crack development of vertical members are key tasks during the RC school building pushover test

Because there are no obvious cracks in the columns of the second floor and elastic deformation is maintained, this study focuses on the importance of the masonry infill and openings for an RC school building. Consequently, only Frame B's and Frame C's failure modes of columns in the

first floor and the crack development of vertical members of specimen MI are examined, as shown in Figs. 16 and 17.

In Figs. 16 and 17, the columns B2 to B6 of Frame B and C2 to C6 of Frame C, which both sides of the columns were adjacent to brick wall piers, displayed diagonal shear cracking patterns. The others, such as column B1, B7, C1, and C7, were flexural failures.

For the span with an opening ratio lower than 40% (Fig. 16), diagonal shear cracks were significantly observed in the brick wall piers adjacent to the columns.

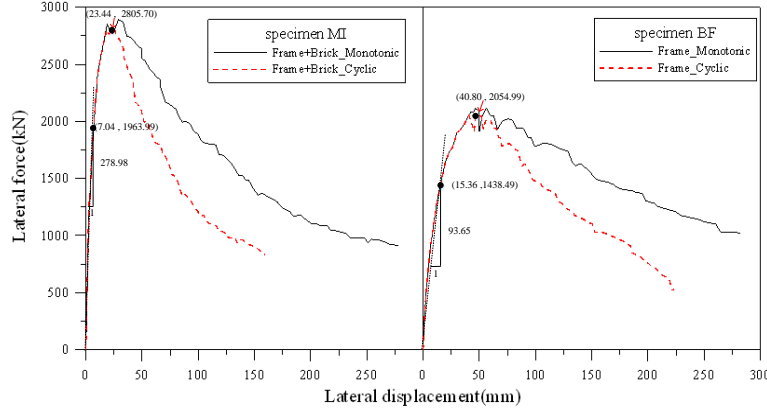


Fig. 18 Overall capacity curves of specimen MI and specimen BF

These diagonal cracks included sliding cracks of horizontal bed-joints and splitting cracks of vertical mortar joints, as well as split of bricks. Even for the span with opening ratio more than 40% (Fig. 17), the diagonal shear cracking patterns could also be found in the brick wall piers. This means that the lateral strength of the brick wall piers of the span with opening ratio more than 40% is still essential.

The final purpose of the field test is to obtain the base shear versus roof displacement (hereinafter referred to as the capacity curve) for specimen MI and specimen BF, as shown in Fig. 18. In Fig. 18, the solid lines are the capacity curves of the in-situ monotonic pushover tests of specimen MI (left-hand) and specimen BF (right-hand). In addition, because seismic force is repeatedly applied to the structure, to truly grasp the response of school buildings during earthquakes, in-situ monotonic pushover tests and in-situ cyclic pushover tests were applied on other school buildings by NCREE (Weng *et al.* 2008). A formula, in accordance with the results of in-situ cyclic pushover tests was derived to convert the capacity curves of the in-situ monotonic pushover tests into that of the in-situ cyclic pushover tests. The modification principle is as follows:

- When  $\Delta_{RF}^{MON} \leq \Delta_{RF,0.97V_{bs,max}^{MON}}$ , then  $V_{bs}^{CYC} = V_{bs}^{MON}$  and  $\Delta_{RF}^{CYC} = \Delta_{RF}^{MON}$ . Here,  $\Delta_{RF}^{MON}$  is the roof displacement corresponding to the base shear of the in-situ monotonic pushover tests,  $\Delta_{RF,0.97V_{bs,max}^{MON}}$  is the roof displacement corresponding to 0.97 times the maximum base shear of the in-situ monotonic pushover tests,  $\Delta_{RF}^{CYC}$  is the roof displacement of the in-situ cyclic pushover tests,  $V_{bs,MON}$  is the base shear of the in-situ monotonic pushover tests,  $0.97V_{bs,max}^{MON}$  is the base shear corresponding to 0.97 times the maximum base shear of the in-situ monotonic pushover tests, and  $V_{bs}^{CYC}$  is the base shear of the in-situ cyclic pushover tests.
- When  $\Delta_{RF,0.97V_{bs,max}^{MON}} < \Delta_{RF}^{MON}$ , then  $V_{bs}^{CYC} = \min(V_{bs}^{MON}, 0.97V_{bs,max}^{MON})$  and  $\Delta_{RF}^{CYC}$  needs to be corrected using formula (1)

$$\Delta_{RF}^{CYC} = \frac{\Delta_{RF,0.97V_{bs,max}^{MON}} + (\Delta_{RF}^{MON} - \Delta_{RF,0.97V_{bs,max}^{MON})}{2} \quad (1)$$

According to this principle, the capacity curve of an in-situ monotonic pushover tests can be converted into capacity curve of an in-situ cyclic pushover test, shown as dashed lines in Fig. 18. The value of the maximum base shear of each test's capacity curve is marked in the graphs. This study also defines the secant stiffness of the rising part of the capacity curve corresponding to 0.7 times the maximum base shear to be the initial stiffness of the specimen MI and specimen BF. It can be seen from Fig. 18 that when specimen BF is filled with a brick wall, then the overall lateral force of the school building will increase by 1.36 times and the initial stiffness will increase by 3 times. It can be seen that a brick wall can increase the lateral force and initial stiffness of a school building, and this observation is the same as that made by Fiorato *et al.* (1970). The lateral force and initial stiffness of the specimen MI and specimen BF in the in-situ cyclic pushover tests will be compared with the analysis results later in this article.

### 3. Simplified analysis of pushover tests

The model for evaluating a masonry infilled RC frame with openings in ASCE/SEI 41-17 (ASCE 2017) was proposed by Andreas Stavridis (2009). In the 2017 version, Stavridis *et al.* (2017) not only substantially updated the calculations of a masonry infilled RC frame with openings but also proposed a capacity curve. The proposed model was validated by the test of three-story, two-span planar RC frame (Stavridis *et al.* 2012). Each story of the planar RC frame contains two masonry infill walls, one without openings, one with openings. The evaluation model could calculate the capacity curves of a masonry infilled RC frame with and without openings on each level. Superimposing the capacity curves of each level can produce the capacity curve of the whole frame. The analysis results can be compared with test results. This superposition method resembles the simplified pushover analysis conducted in Taiwan (Tu *et al.* 2009).

Simplified pushover analysis (Tu *et al.* 2009) is a pushover analysis that allows manual solution of the failure mode of members and complete capacity curve of a structure without requiring commercial software.

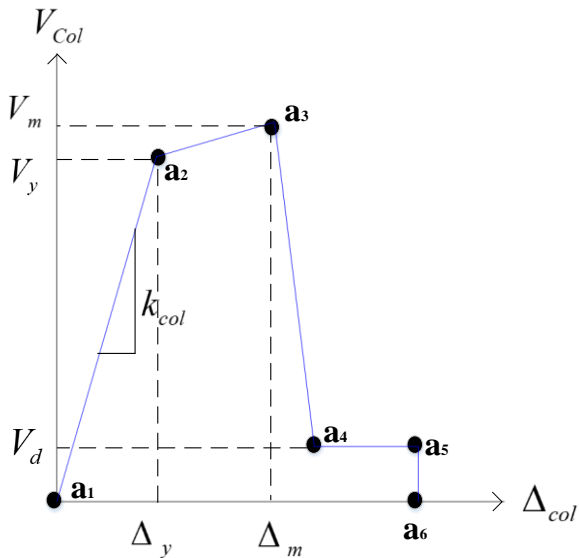


Fig. 19 Capacity curve for a column from the ASCE/SEI 41-17 evaluation model

This method is suitable for low-rise buildings in Taiwan and its consistency has been verified through *in-situ* pushover tests of school buildings in Taiwan (Chung *et al.* 2012). The following subsections will introduce the basic hypothesis and analysis procedure of the simplified pushover analysis.

### 3.1 Basic hypothesis of simplified pushover analysis

Early buildings in Taiwan, regardless of whether they are houses or schools, were mostly low-rise (i.e., below five floors) RC buildings with masonry infill and openings. From field observations after the Chi-Chi earthquake, the horizontal members (e.g., beams and slabs) along the long direction of these low-rise RC buildings were only damaged slightly, while the vertical members (e.g., columns and masonry infill walls with openings) always caused the main damage and collapse of building. The collapsed buildings were damaged in a weak-column strong-beam mode.

We can assume that the existing low-rise building will resemble a shear type frame when it subjected to a lateral earthquake loading. The shear type frame is a building frame with rigid diaphragm on each floor. None of the joints on the rigid diaphragm will have relative displacements. Therefore, the relative displacements of two top and down floors can represent the lateral deformation of vertical members between the two floors. In this study, displacement of central mass of the floors was adopted to represent the lateral deformation of vertical members in the evaluated story.

Because lateral stiffness of the vertical members is not the same, the ultimate lateral strength of the vertical members would not simultaneously achieve under the same displacement of the story.

Story shear strength of the evaluated story could be calculated by superposing the lateral strength of all the vertical members in the story, in which the lateral strength of each member could be determined in accordance with the

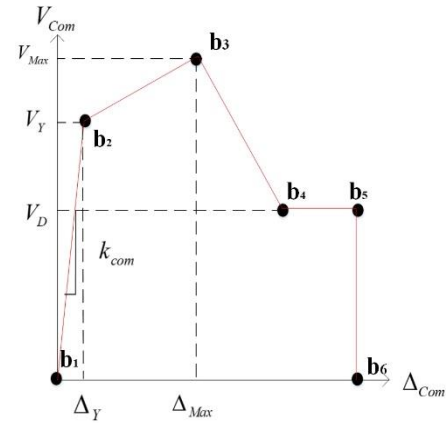


Fig. 20 Capacity curve for a composite column from the ASCE/SEI 41-17 evaluation model

backbone curve of the lateral strength vs deformation.

If the low-rise RC building conforms to the basic features (e.g., a weak-column strong-beam failure mode during an earthquake), then the capacity curve of the structure can be obtained through simplified pushover analysis.

### 3.2 Capacity curve of vertical members of each floor

This paper uses ASCE/SEI 41-17 (ASCE 2017) as the main evaluation model. From the above, it is known that the main damage to school buildings after *in-situ* pushover tests is concentrated in columns and masonry infill walls with openings along the corridor direction of the building, so the vertical members determine the seismic capacity of a structure. Therefore, the first step of simplified pushover analysis is to find the capacity curves of the vertical members of each floor. Taking specimen MI as an example, there are two types of vertical members along the corridor direction of the school buildings. The evaluation model of ASCE/SEI 41-17 (ASCE 2017) gives a capacity curve for a column, as shown in Fig. 19.

In Fig. 19,  $a_1$  is the origin point,  $a_2$  is the yield bending moment point,  $a_3$  is the ultimate point of the bending moment,  $a_4$  is the residual strength point,  $a_5$  is the ultimate displacement point, and  $a_6$  is the failure point. To reduce the length of the article, only the maximum base shear and initial stiffness are compared. Therefore, only the ASCE/SEI 41-17 (ASCE 2017) column evaluation model's formula for the maximum base shear and initial stiffness is listed below. Because this study's hypothesis is that a school building is a shear type frame, the column is subjected to double curvature bending under an earthquake, so the yield strength  $V_y$  and ultimate strength  $V_m$  of the column are both the result of the summation of the moments at the top and bottom of the column divided by the clear height of the column. Furthermore, because the cross-section details of the top and the bottom of the column are the same, the same bending moment strength can be expected for the top and bottom of the column. Consequently, the moment capacity of the column is double

curvature bending moment for the analysis.

Therefore,  $V_y = \frac{2M_y}{H_n}$  and  $V_m = \frac{2M_n}{H_n}$ , where  $M_y$  and  $M_n$  are the yield and ultimate bending moments of the column, which can be found from the analysis of the cross-section of the column. Furthermore, for the sake of being conservative and to simplify the calculation, strain hardening of longitudinal reinforcement is not considered when calculating  $M_n$ .

The initial stiffness of the column evaluation model is  $k_{col} = \frac{12(\gamma EI)_{col}}{H_n}$ , where  $(\gamma EI)_{col}$  is the flexural rigidity of the column sections and  $\gamma_{col}$  is the reduction factor of the column sections. According to ASCE/SEI 41-17 (ASCE 2017), if the design axial load of a column is greater than  $0.5A_g f'_c$ , then  $\gamma = 0.7$ ; if it is smaller than  $0.1A_g f'_c$ , then  $\gamma = 0.3$ ; and if the axial load is in between, then  $\gamma$  is obtained according to interpolation. Here,  $A_g$  is the total cross-section area of the column. For both specimen MI and specimen BF in this study, the design axial load of a column  $N$  is less than  $0.1A_g f'_c$ , so  $\gamma = 0.3$ . In addition,  $E_{col} = 4700\sqrt{f'_c}$  and  $I_{col}$  is the moment of inertia of gross concrete or a masonry section about the centroidal axis, neglecting reinforcement. The coordinates of  $a_1 (0,0)$ ,  $a_2 (\Delta_y = \frac{V_y}{k_{col}}, V_y)$ , and  $a_3 (\Delta_m, V_m)$  in Figure 19 can be established from the previous formula and parameters. Moreover,  $\Delta_m$ ,  $a_4$ ,  $a_5$ ,  $a_6$ , and other coordinate values can be obtained from Table 10-8 of ASCE/SEI 41-17 (ASCE 2017).

Another vertical member of specimen MI is the masonry infill walls with openings. ASCE/SEI 41-17 (ASCE 2017) states that masonry infill walls with openings can not only be simulated with a diagonal compression strut but can also be combined with the columns on both sides into a masonry infilled RC frame, and can then be analyzed as a composite cantilever column. The ASCE/SEI 41-17 (ASCE 2017) evaluation model's capacity curve of a composite cantilever column is shown in Figure 20.

In Figure 20,  $b_1$  is the origin point,  $b_2$  is the yield bending moment point,  $b_3$  is the ultimate bending moment point,  $b_4$  is the residual strength point,  $b_5$  is the ultimate displacement point, and  $b_6$  is the failure point. It should be noted that ASCE/SEI 41-17 (ASCE 2017) uses the ratio of shear strength to flexural strength of a column,  $\frac{V_n}{V_m}$ , to classify the frame as ductile or nonductile.

The shear strength of the column  $V_n$  can be calculated with the following formula:

$$V_n = k_{nl} \left[ \alpha_{col} \left( \frac{A_{st} f_{yt} d_{col}}{s} \right) + \lambda \left( \frac{0.5\sqrt{f'_c}}{M_n/V_y d} \sqrt{1 + \frac{N}{0.5A_g \sqrt{f'_c}} f'_c} \right) 0.8A_g \right] \quad (2)$$

If the displacement ductility requirement  $\mu_d \leq 2$ , then  $k_{nl} = 1$ . If the displacement ductility requirement  $\mu_d \geq 6$ , then  $k_{nl} = 0.7$ . If the displacement ductility requirement  $2 \leq \mu_d \leq 6$ , then  $k_{nl}$  is obtained by interpolation. Here,  $\alpha_{col}$  is the reduction factor of column strength; if  $\frac{s}{d_{col}} \leq 0.75$ , then  $\alpha_{col} = 1$ . If  $\frac{s}{d_{col}} \geq 1$ , then  $\alpha_{col} = 0$ , and when  $0.75 \leq \frac{s}{d_{col}} \leq 1$ ,  $\alpha_{col}$  can be found by interpolation. Next,

$s$  is the spacing of hoops;  $d_{col}$  is the effective depth of a column cross-section;  $A_{st}$  is the transverse reinforcement's cross-section area within the spacing of a hoop ( $s$ );  $f_{yt}$  is the yield strength of a hoop, and when the concrete is normal-weight concrete, then  $\lambda = 1$  and  $2 \leq \frac{M_n}{V_y d} \leq 4$ .

An infill with openings is classified by ASCE/SEI 41-17 (ASCE 2017) as strong or weak according to the  $\frac{K_{inf}}{K_c}$  ratio. Here,  $K_{inf}$  is the lateral stiffness of the infill with openings, calculated by the following equation:

$$K_{inf} = \frac{1}{\left( \frac{1}{K_{inf f}} + \frac{1}{K_{inf s}} \right)} \quad (3)$$

Where  $K_{inf f} = \frac{3E_m I_{inf}}{h_{inf}^3}$  is the flexural stiffness of an infill with openings;  $E_m = 550f'_m$  is the brick wall's elastic modulus;  $f'_m$  is the compressive strength of masonry prisms;  $I_{inf}$  is the moment of inertia of a gross masonry section about its centroidal axis;  $h_{inf}$  is the effective height of the infill with openings;  $K_{inf s} = \frac{A_w G_{me}}{h_{inf}}$  is the shear stiffness of the infill with openings;  $A_w$  is the horizontal cross-sectional area of an infill with openings, which is  $A_w = h_{inf}(L_{inf} - L_{op})$ ;  $L_{inf}$  is length of brick wall;  $L_{op}$  is horizontal length of the opening of brick wall. It should be noted that the opening's area of masonry infill does not exceed 40%. Next,  $G_{me} = 0.4E_m$  is the shear modulus of masonry;  $K_c = \frac{3E_{col} I_{col}}{h_{inf}^3}$  is the column's flexural stiffness.

RC frames with masonry infill and openings can be divided into four types. Because different frame types have different lateral forces and lateral displacements, then, before conducting composite cantilever column analysis, the type of masonry infilled RC frame with openings needs to be identified.

According to ASCE/SEI 41-17 (ASCE 2017) Table 11-8, the composite cantilever columns in this paper are all ductile and relatively flexible panels.

Only the maximum lateral force and initial stiffness for the ductile relatively flexible panels for these composite cantilever columns are listed below. ASCE/SEI 41-17 (ASCE 2017) recommends to pick whichever is larger of  $V_1$  and  $V_2$  when finding the maximum lateral force of the ductile relatively flexible panel,  $V_{Max} = Max(V_1, V_2)$ . These can be found using

$$V_1 = P_{inf}^{grav} \times \mu + A_w \times C_{com} \quad (4)$$

$$V_2 = P_{inf}^{max} \times \mu + V_{lc}^{max} \quad (5)$$

where  $P_{inf}^{grav}$  is the gravity load sustained by the infill wall; and  $\mu$  is initial friction coefficient of the infill wall, which can be between 0.3 to 1.6, and can be obtained from the test in accordance with ASTM C1531 (2016). In the study, there were technical problems for sampling of existing masonry infill to conduct the test in accordance with ASTM C1531. Therefore,  $\mu$  was assumed to 0.3 for

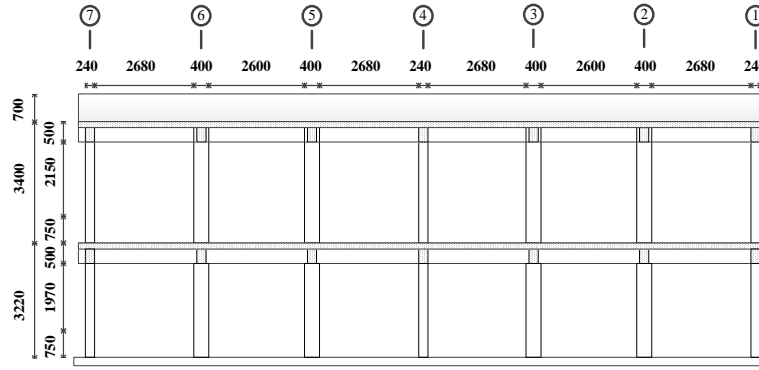


Fig. 21 Six spans of bare frame Frame C of specimen MI

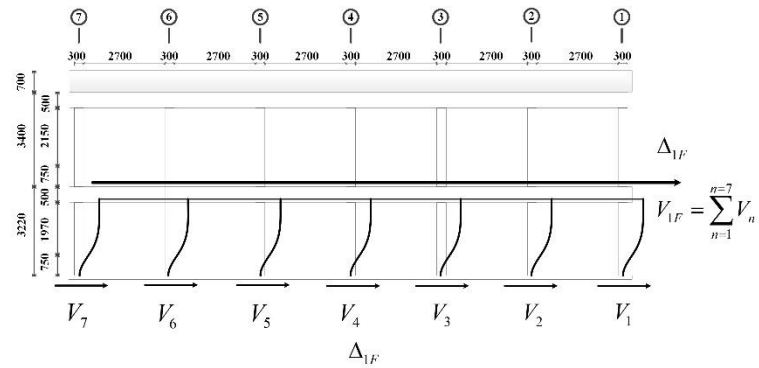


Fig. 22 Lateral strength superposition with synchronous displacement

conservative consideration in the study.

Next,  $A_w$  is the width of the brick wall times the thickness of the horizontal shear stress area. Next,  $C_{com}$  is the test values of cohesion of the brick–mortar interface, which is equal to the shear strength when no axial stress is applied. Because the in-situ pushover test of specimen MI does not have test values for  $C_{com}$ , it will be obtained by an empirical formula. As seen in the relevant literature (Ali1 *et al.* 2012), the empirical formula of  $C_{com}$  is  $C_{com} = 0.0337(f_{mc})^{0.6}$ . It can be seen that  $C_{com}$  is the power of the compressive strength of mortar multiplied by a coefficient. Because the in-situ pushover test is conducted in Taiwan, for the value of  $C_{com}$ , this paper uses the empirical formula of Taiwan's Design and Construction Specifications of Brick Structures for Buildings  $C_{com} = 0.0258(f_{mc})^{0.885}$ . In Eq. (5),  $P_{inf}^{max}$  is the total axial load supported by the infill at a distance equal to half of the column depth from the bottom of the infill when the maximum strength is reached, which can be obtained from ASCE/SEI 41-17 (ASCE 2017) Table 11-9. Next,  $V_{lc}^{max}$  is the shear strength of the leeward column governed by the minimum shear or the flexural capacity of the column, with  $V_{lc}^{max} = V_m$  for ductile frames and  $V_{lc}^{max} = V_n$  for nonductile frames. The initial stiffness of the composite cantilever column is  $k_{com} = (1 - \frac{2A_{op}}{A_{inf}})k_{soild}$ , where  $A_{op}$  is the opening area and  $A_{inf}$  is the total area of a frame with masonry infill, including openings in the infill wall,  $k_{soild} = \frac{1}{(\frac{1}{K_{fl}} + \frac{1}{K_{sh}})}$ ,  $K_{fl} = \frac{3E_{col}I_{ce}}{h_{inf}^3}$ , is the flexural stiffness of

the equivalent composite cantilever column;  $I_{ce}$  is the equivalent moment of inertia of the transformed section;  $h_{inf}$  is the clear height of the infill wall for an individual bay in one story,  $K_{sh} = \frac{A_w G m e}{h_{inf}}$  is the shear stiffness of the equivalent composite cantilever column, so Fig. 20's coordinate values  $b_1$  (0,0),  $b_2$  ( $\Delta_{yield} = 2 \frac{V_{max}}{3k_{com}}$ ,  $\frac{2V_{max}}{3}$ ) and  $b_3$  ( $\Delta_{max}$ ,  $V_{max}$ ) can be established. Coordinates such as  $\Delta_{max}$ ,  $b_4$ ,  $b_5$ , and  $b_6$  can be obtained from ASCE/SEI 41-17 (ASCE 2017) Table 11-9 and Table 11-11. Furthermore, if two RC frames with masonry infill and openings share one column, then the axial load of the column needs to be distributed to two RC frames with masonry infill and openings to avoid overestimating the axial load that the two are bearing.

### 3.3 Simplified pushover analysis steps

Because this study considers specimen MI and specimen BF as shear type frame, the slab of the floor and beam connected together can be regarded as rigid, so the building will only move horizontally during movement. The vertical members that are connected to the slab of the floor and beam, such as the column and masonry infill and openings, would also move horizontally. Therefore, the displacement of a story can be regarded as equal to the displacement of the vertical members in that floor. Therefore, if the lateral force of the vertical members in each floor are superimposed corresponding to the same lateral displacement of the floor, then the lateral force of the story can be obtained. This superposition may also be called

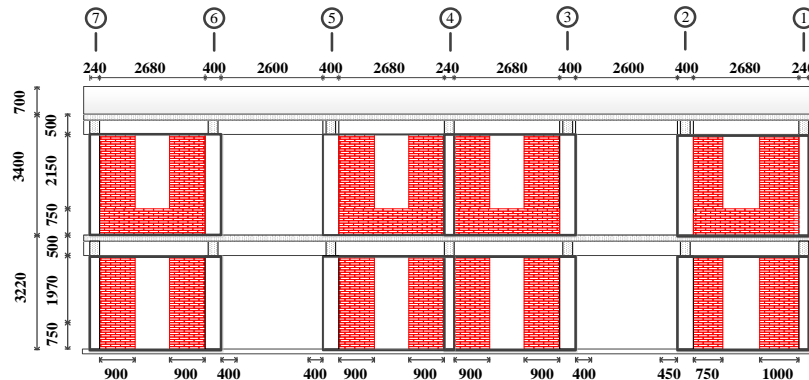


Fig. 23 Composite column frame diagram of Frame B of specimen MI

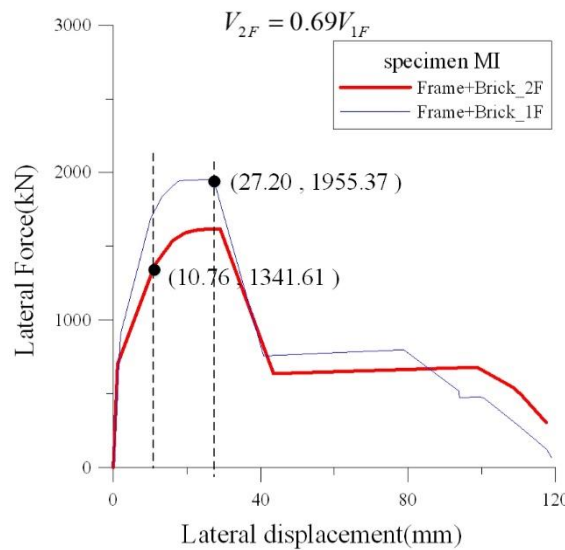


Fig. 24 Capacity curves of the first and second floors of specimen MI

lateral force superposition via consistent displacement. Taking a school building in specimen MI as an example, the second floor and roof floor of Frame A and the second floor of Frame D are bare frames. In addition, Frame C is a masonry infilled RC frame with openings, but it is considered an ineffective member according to ASCE/SEI 41-17 (ASCE 2017) because the opening area of the masonry infill is greater than 40% (Fig. 17). Therefore, the second floor and roof floor of Frame C were simulated by bare frames with six spans, as shown in Fig. 21.

As can be seen in Fig. 22, when the lateral displacement of the first floor of Frame A is  $\Delta_{1F}$ , all vertical members in the first floor of Frame A also deform with  $\Delta_{1F}$ . Therefore, the lateral strength of the first floor can be the summation of lateral strength of all vertical members of the first floor of Frame A. —i.e.,  $V_{1F} = \sum_{n=1}^{n=7} V_n$ . According to this, each bare frame’s capacity curve can be worked out.

Therefore, they are ineffective members according to ASCE/SEI 41-17 (ASCE 2017). The masonry infilled RC frame with openings consists of vertical members, such as

columns and masonry infill and openings.

ASCE/SEI 41-17 (ASCE 2017) states that the column and brick wall can be combined into a composite cantilever column for analysis. Therefore, Frame B’s first floor and second floor would have four composite cantilever columns, respectively. The composite cantilever column frame diagram is shown in Fig. 23.

The second step of the simplified pushover analysis is to calculate the capacity curve of each story. The first floors of Frame A and Frame C each have seven columns. Frame D has three columns. Frame B has four composite cantilever columns.

Therefore, the first floor of specimen MI has 21 vertical members. For each vertical member, there are six displacement points determined in accordance with Figs. 19 and 20. Consequently, 126 ( $6 \times 21$ ) displacement points will be indicated for the synchronous displacement of the first story.

Then, lateral strength of each vertical member correspondence with the 126 synchronous displacement can

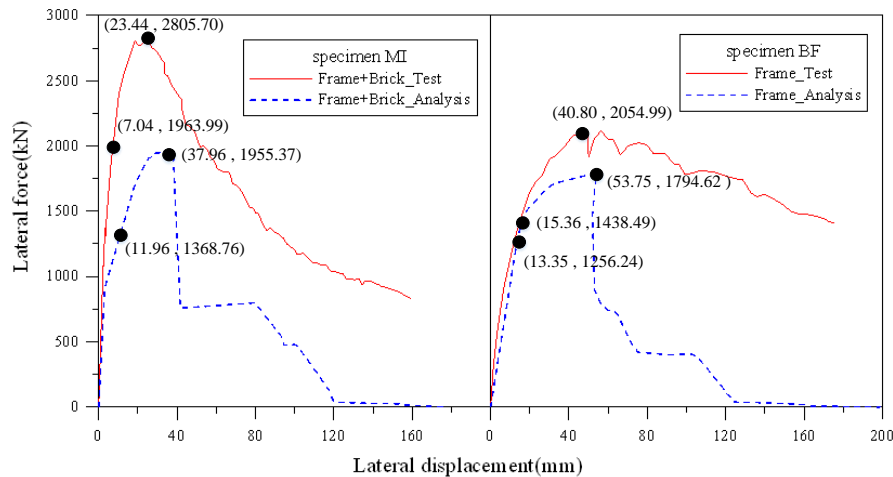


Fig. 25 Capacity curves of test and analysis for specimen MI and specimen BF

be determined in accordance with the capacity curve as shown in Figs. 19 or 20. Eventually, the lateral strength of the vertical members correspondence with the 126 synchronous displacement are superimposed to obtain the capacity curve of the first floor of specimen MI, which is shown in Fig. 24 by the thin line. The same procedure can be used to obtain the capacity curve of the second floor, as shown in Fig. 24 by the thick line.

The third step of the simplified pushover analysis is to find the capacity curve of the RC building.

The lateral force of the first story is the base shear of the RC school building  $V_{bs}$  ( $V_{1F} = V_{bs}$ ). When the lateral displacement of the first story of the building is  $\Delta_{1F}$ , the lateral force is  $V_{1F}$ . The second floor's corresponding lateral force,  $V_{2F}$ , can be determined according to the earthquake's inverted-triangle distribution equation in the Seismic Design Specifications and Commentary of Buildings in Taiwan (Construction and Planning Agency Ministry of the Interior 2011)

$$V_{2F} = \frac{W_{RF} h_{RF}}{W_2 h_2 + W_{RF} h_{RF}} \times V_{1F} \quad (6)$$

where  $W_2$  and  $W_{RF}$  are the weight of lump mass in the second-floor and in the roof-floor, respectively;  $h_2$  and  $h_{RF}$  are the height of the second-floor and roof-floor from the base level, which are 3220 mm and 6620 mm, respectively. Once  $V_{2F}$  is determined, the corresponding displacement of the second floor  $\Delta_{2F}$ , can be calculated in accordance with the capacity curve of the second floor. Eventually, by superimposing  $\Delta_{1F}$  and  $\Delta_{2F}$ , the roof displacement  $\Delta_{RF}$  of specimen MI can be calculated:

$$\Delta_{RF} = \Delta_1 + \Delta_2 \quad (7)$$

For example,  $W_2$  of Specimen MI and Specimen BF are 2,528.05kN and 2,591.75kN, respectively.  $W_{RF}$  of Specimen MI and Specimen BF are 2,687.69kN and 2,354.14kN, respectively.  $h_2$  of Specimen MI and Specimen BF are both 3,220 mm,  $h_{RF}$  of Specimen MI and Specimen BF are both 6,620 mm. Therefore,  $V_{2F} =$

$0.69V_{1F}$  in accordance with equation (6). For example, it can be seen in Fig. 24 that, when  $V_{1F}$  is 1,955.37kN,  $V_{1F}$ 's corresponding  $\Delta_1$  is 27.20 mm. At this time,  $V_{2F}$  is 1,341.61kN, and by checking the capacity curve of the second floor in Fig. 24,  $V_{2F}$ 's corresponding  $\Delta_2$  is found to be 10.76 mm. By adding  $\Delta_1$  and  $\Delta_2$ , the roof displacement RF can be found to be 37.96 mm. According to this, **specimen MI**'s capacity curve can be found, as shown on the left-hand side in Fig. 25.

To reduce the length of this article, only the maximum base shear of the capacity curve and the initial stiffness are compared. As shown in Fig. 25, the calculated maximum base shear of specimen MI and specimen BF are 69.69% and 87.33% of the test value, respectively. The analysis results are more conservative than the test values.

In addition, the ascending section of the capacity curve corresponds to 0.7 times the maximum base shears, which are 1368.76kN and 1256.24kN, respectively. The corresponding lateral displacements are 11.96 mm and 13.35 mm. Therefore, the calculated structure stiffnesses are 41.04% and 100.49% of the test value. The initial stiffness test result of specimen MI is more conservative compared to the test value. The initial stiffness of specimen BF is closer to the test value.

The reason why the analysis values for the maximum base shear and initial stiffness of specimen MI are more conservative than the test values is that the source of the error may be the column evaluation model or the masonry infilled RC frame with openings evaluation model or a calculation error.

According to the results of the maximum base shear analysis of specimen BF, this error may arise because the strain hardening of the longitudinal reinforcement is not considered when calculating  $M_n$ . The source of error of initial stiffness comes from the reduction factor of the column cross-section (EI) (this study considers EI to be 0.3). Because the analysis results for specimen BF are not bad, the possibility of calculation error due to being unfamiliar with the ASCE/SEI 41-17 (ASCE 2017) column evaluation model can be ruled out.

Next, the composite cantilever column evaluation model

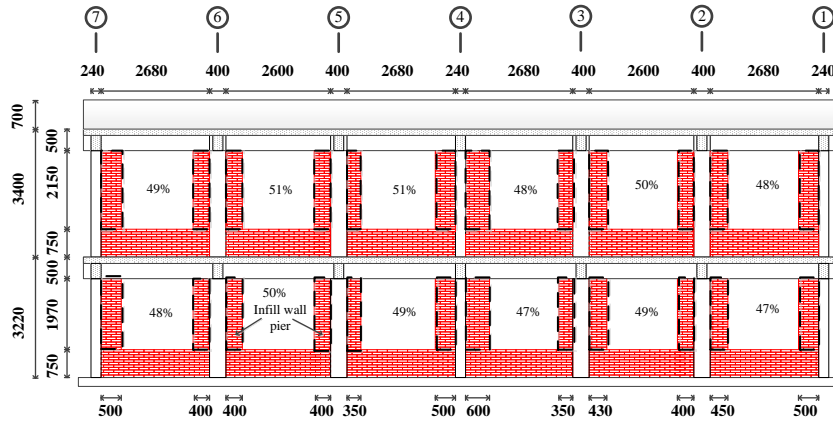


Fig. 26 Simulated masonry infill with an opening ratio more than 40%

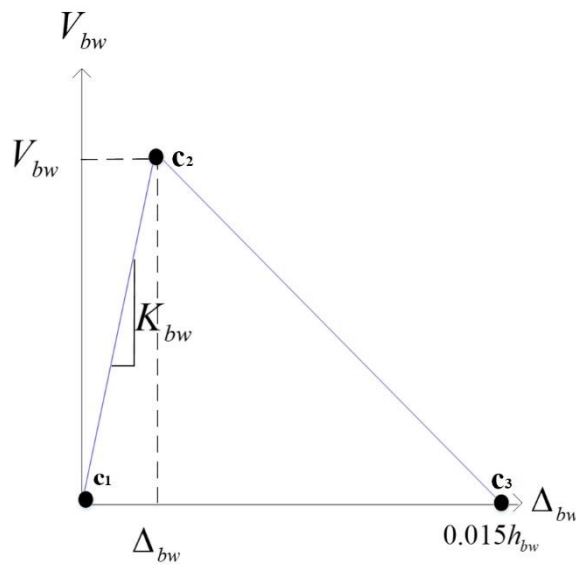


Fig. 27 Evaluation model for brick walls

is reviewed for calculation error. For maximum lateral force, Eq. (4) shows the column lateral resistance can be ignored and Eq. (5) shows the column can provide lateral resistance, respectively.

However, as can be seen in Fig. 16, the columns displayed diagonal shear cracking patterns, it means the column can provide shear resistance. And in this study, the calculation of lateral force of the composite cantilever column is controlled by Eq. (5). Therefore, we can confirm that calculation error due to being unfamiliar with the ASCE/SEI 41-17 (ASCE 2017) composite cantilever column evaluation model can be ruled out.

Therefore, the reason why the maximum base shear analysis value of specimen MI is more conservative than the test value is possibly because ASCE/SEI 41-17 (ASCE 2017) ignores masonry infill walls with an openings ratio of more than 40%.

This study suggests that the behavior of masonry infill walls with openings ratios greater than 40% should be simulated moderately.

#### 4. Proposed evaluation model of masonry infill with opening ratio over 40%

ASCE/SEI 41-17 (ASCE 2017) states that the contribution of the masonry infill can be ignored when the openings ratio of a masonry-infilled wall is greater than 40%. However, the results of the analysis of specimen MI show that, if we only consider the masonry infill wall with openings ratio less than 40%, then the analysis value of maximum base shears and initial stiffness are 69.69% and 41.04, respectively, of the test.

Therefore, it is necessary to simulate the behavior of a masonry infill wall when the openings ratio is more than 40%.

In Fig. 17, when the openings ratio of a masonry infill wall is greater than 40%, the cracks develop in an almost diagonal direction and are concentrated above the windowsill. This means the range of windowsill are damaged slightly.

Therefore, in analysis of the frame C of specimen MI, we propose that the columns and the brick infills above the

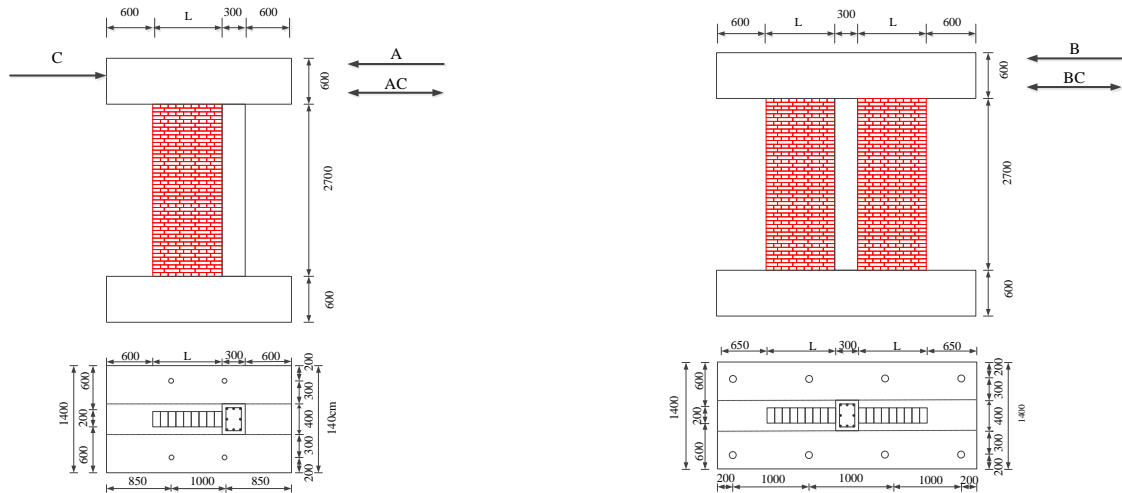


Fig. 28 Plans and Elevations of specimen A, AC, C, B, and BC

Table 5 Material parameters of specimens A, AC, C, B, and BC

specimen	$f'_c$ (MPa)	$f_{yl}$ (MPa)	$f_{yt}$ (MPa)	$f'_m$ (MPa)	$f_{mc}$ (MPa)	$C_{com}$ (MPa)
A	30.4	439.2	318.9	17.4	15.5	1.54
AC	33.6	490.5	400.3	19.4	13.9	1.35
C	30.9	490.5	400.3	19.4	13.9	1.35
B	30.4	439.2	318.9	17.4	15.5	1.54
BC	32.4	490.5	400.3	19.4	13.9	1.35

windowsill are simulated separately instead of using composite cantilever columns. Consequently, the simulated brick infill of frame C is shown in Fig. 26.

In Fig. 26, to simulate the captive effect of windowsill, the effective height of columns is determined from windowsill to beam bottom. Moreover, the considered infill wall piers as shown in Fig. 26 can be evaluated by an unreinforced masonry (URM) wall. The study proposed to evaluate the URM in accordance with ASCE/SEI 41-17 (ASCE 2017).

ASCE/SEI 41-17 (ASCE 2017) states that URM's lateral stiffness is  $K_{bw} = \frac{1}{\frac{1}{K_{bwf}} + \frac{1}{K_{bws}}}$ , where  $K_{bwf} = \frac{3EmI_{bw}}{h_{bw}^3}$

is the flexural stiffness provided for a brick wall and  $K_{bws} = \frac{AwGme}{h_{bw}}$  is the shear stiffness provided for brick wall.

Here,  $I_{bw}$  is the cross-section moment of inertia of the brick wall and  $h_{bw}$  is the effective height of the brick wall. In addition, the maximum lateral force of a brick wall is

$V_{bw} = \frac{Aw[0.75(0.75C_{com} + \frac{P_D}{Aw})]}{1.5}$ , where  $P_D$  is the axial load of a brick wall.

ASCE/SEI 41-17 (ASCE 2017) proposed a capacity curve for URM as shown in Figure 27.

This study first verifies the consistency of the above brick wall evaluation model with the pushover tests (Tu *et al.* 2020, Tu *et al.* 2011, Lo, T.Y. 2010, and Lin, B.C. 2011) of the existing five columns with brick walls on one side or both sides.

Specimens A, AC, and C of the five tests are typical columns with an infill wall pier on one side, while specimens B and BC are typical columns with infill wall

piers on both sides. The testing variables mainly examine the seismic behavior of a column with infill wall piers on one or both sides, and it considers infill wall piers of different widths, as well as a monotonic or cyclic applied lateral load.

The plans and elevations of specimens A, AC, C, B, and BC are shown in Fig. 28.

The vertical loadings of specimens A, AC, C, B, and BC are 322.6kN, 316.6kN, 325.3kN, 333.7kN and 325.4kN, respectively. In these five tests, the columns have a consistent cross section of 300 mm x 400 mm. The dimension of the infill wall piers is 900mm wide, 2700mm high, and 200 thick. The infill was laid by solid clay bricks that are 200mm long, 95mm wide, and 53mm thick.

The material parameters of column and brick wall are shown in Table 5.

The capacity curves for the analysis and test results are plotted in Fig. 29. The analytical capacity curves are superimposed by the capacity curves of the column and the infill wall piers in accordance with the column model and URM model of ASCE/SEI 41-17 (ASCE 2017).

The evaluation results show that the analysis will underestimate the maximum base shear and the initial stiffness compared to the test values when only considering the contribution of the columns; as shown in Fig. 29 by black dash lines.

When the infill wall piers are considered by URM, the maximum base shear of analysis for specimens A, AC, C, B, and BC are 71.67%, 84.65%, 70.91%, 66.62%, and 62.54% of the test values, respectively; as shown in Fig. 29 by blue-dashed lines. Therefore, if the infill wall piers are taken into consideration, then the analysis result will exhibit a

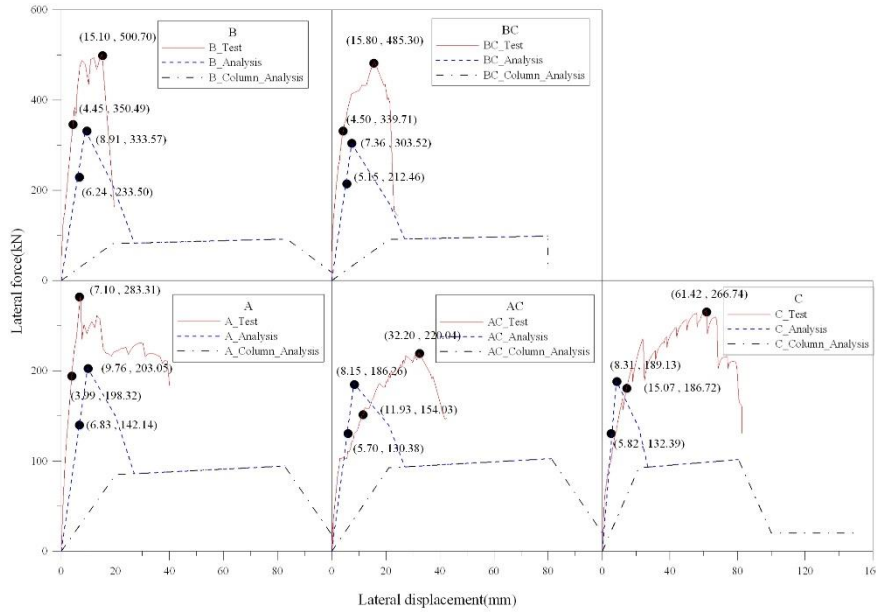


Fig. 29 Verification for the evaluation model of the infill wall piers

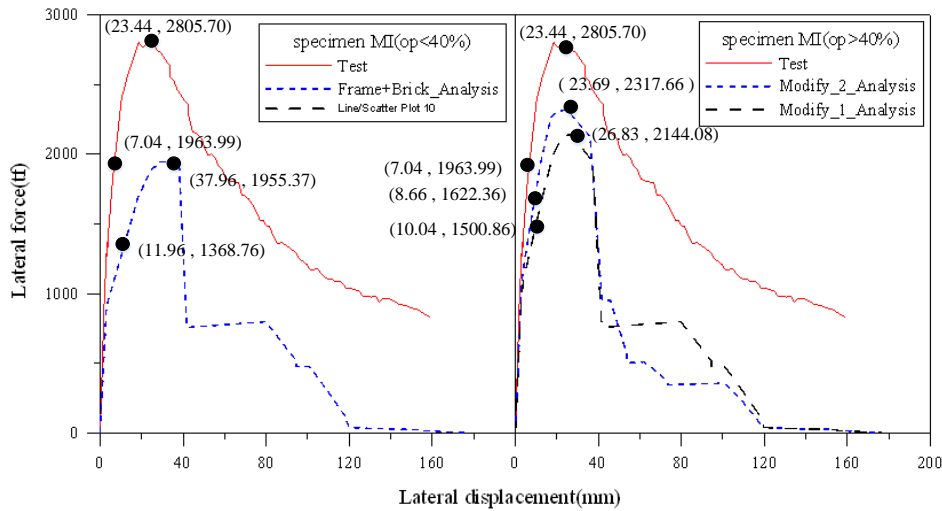


Fig. 30 The capacity curve of the masonry infilled wall with openings ratio greater than 40%

significant improvement that is more consistent with the behavior of the tests and is still conservative compared to the test values.

The initial stiffnesses, which in the ascending section of the capacity curve corresponds to 0.7 times the maximum base shear, for specimens A, AC, C, B, and BC are 41.84%, 177.11%, 183.76%, 47.58%, and 54.62% of the test values, respectively. Therefore, if the infill wall piers are taken into consideration, then the predicted initial stiffness will be significantly improved. Consequently, the proposed evaluation model of the column with infill wall piers can feasibly be performed.

Next, we will move on to predict the capacity curve for specimen MI by simplified pushover analysis. The column

evaluation model from ASCE/SEI 41-17 (ASCE 2017) is adopted for frames A and D of specimen MI. The composite cantilever column evaluation model from ASCE/SEI 41-17 (ASCE 2017) is applied for frame B. The column model combined with the URM evaluation model are used for the masonry infilled RC frame with an opening ratio over 40% frame C. Moreover, to simulate the contribution of a windowsill, the effective height of columns and infill wall piers will be shortened (i.e., from windowsill to beam bottom).

The predicted capacity curves for specimen MI are plotted in Fig. 30. In the right-hand of Fig. 30, modify 1 analysis represents consideration of masonry infill with an opening ratio of over 40% in frame C. Moreover, modify 2

Table 6 Comparison of strength values from field tests and analysis

Test unit	Maximum strength from tests (kN)	Corresponding displacement of maximum strength from tests (mm)	Maximum strength from analysis (kN)	Corresponding displacement of maximum strength from analysis (mm)	Strength difference (kN)	Strength ratio (%)
Bare-frame frame	2054.99	40.8	1794.62	53.75	260.37	87.33%
Specimen MI	2805.7	23.44	1955.37 (ignoring infills with openings ratio greater than 40%)	37.96	850.33	69.69%
			2317.66 (considering infills with openings ratio greater than 40%)	23.69	488.04	82.60%

Table 7 Comparison of stiffness values from field tests and analysis

Test unit	Initial stiffness from tests (kN/mm)	Initial stiffness from analysis (kN/mm)	Stiffness difference (kN/mm)	Stiffness ratio (%)
Bare-frame frame	93.65	94.11	-0.46	100.49%
		114.48 (ignoring infills with openings ratio greater than 40%)	164.50	41.04%
Specimen MI	278.98	187.27 (considering infills with openings ratio greater than 40%)	91.71	67.13%

analysis represents consideration of masonry infill with an opening ratio of over 40%, as well as the shortened effective height of the columns in frame C.

The modify 1 analysis finds that the maximum base shear of specimen MI is 2144.08kN, which is 76.42% of the test value. Therefore, the contribution of the maximum base shear of the masonry infill wall with an opening ratio greater than 40% is 188.71kN (2144.08-1955.37).

The modify 2 analysis finds that the maximum base shear of specimen MI is 2317.66kN, which is 82.60% of the test value. Therefore, the contribution of the maximum base shear of the short column is 173.58kN.

These results for the maximum base shear are more conservative than the test value. The test results are summarized in Table 6.

It is worth noting that when we considered a masonry infill wall with an opening ratio greater than 40% and the short column in frame C, the predicted maximum base shear increased from 69.69% to 82.60% of the test value.

When compared with the masonry infill wall with an opening ratio greater than 40% and not considering the short column of frame C, the initial stiffness increases from 41.04% to 53.58% of the test value. When we consider the short column effect, the initial stiffness increased from 41.04% to 67.13% of the test value. Therefore, the proposed method for masonry infill with a large opening ratio can be used to predict the seismic behavior of a masonry infilled RC frame with openings. The result for the initial stiffness is summarized in Table 7.

## 5. Conclusions

- This study reports two in-situ pushover tests of a full-

size school building with a two-story, six-span RC frame. The two tests can be used to compare the seismic behavior of a RC frame with and without masonry infill. The test results are a significant contribution to our understanding of the seismic behavior of full-size structures by an in-situ test.

- It can be seen from the in-situ pushover test in the study that when RC frames are filled with brick walls (e.g., specimen MI), the overall maximum base shear of the RC school building will increase by 1.36 times and the initial stiffness will increase 3 times. Therefore, masonry infill walls with openings cannot be ignored when conducting analysis because it is obvious that the masonry infill contributes to the overall maximum base shear and initial stiffness.

- The column evaluation model of ASCE/SEI 41-17 is verified by the in-situ pushover test of specimen BF. Consequently, the maximum base shear of the school building is 87.33% and the initial stiffness is 115.49% of the test value. Therefore, the analysis result is very close to the test result.

- The composite cantilever column evaluation model for masonry infill by ASCE/SEI 41-17 is verified by the in-situ pushover test of specimen MI. Consequently, the maximum base shear of the RC school building is 69.69% of the test value. The initial stiffness is 58.47% of the test value. The reason for this conservative result is that ASCE/SEI 41-17 ignores masonry infill when the opening ratio is greater than 40%. Therefore, masonry infill walls with an opening ratio greater than 40% should be included in the analysis.

- This study proposed a procedure to simulate masonry infill with a large opening ratio. The infill walls can be evaluated by URM in accordance with ASCE/SEI 41-

17. Meanwhile, the effective height of captive columns with a windowsill also needs to be shortened. Consequently, the maximum base shear of the predicted capacity curve (e.g., specimen MI) increases from 69.69% to 82.60%, and the initial stiffness also increases from 58.47% to 92.89%. Therefore, the proposed method for masonry infill with a large opening ratio can predict the seismic behavior of a masonry infilled RC frame with openings.

## References

- Ahani, E., Mousavi, M.N., Ahani, A. and Kheirollahi, M. (2019), "The effects of amount and location of openings on lateral behavior of masonry infilled RC frames", *KSCE J. Civil. Eng.*, **23**(5), 2175-2187. <https://doi.org/10.1007/s12205-019-0714-x>.
- Aknouche, H., Airouche, A. and Bechtoula, H. (2019), "Effect of masonry infilled panels on the seismic performance of a R/C frames", *Earthq. Struct.*, **16**(3), 329-348. <https://doi.org/10.12989/eas.2019.16.3.329>.
- Al-Chaar, G., Lamb G.E. and Abrams, D.P. (2003), "Effect of openings on structural performance of unreinforced masonry infilled frames", *Content uploaded by Ghassan Al-Chaar*. <https://www.researchgate.net/publication/265562695>.
- Ali, Q., Badrashi, Y.I., Ahmad, N., Alam, B., Rehman, S. and Banori, F.A. (2012), "Experimental investigation on the characterization of solid clay brick masonry for lateral shear strength evaluation", *Int. J. Earth. Sci. Eng.*, **5**(4), 782-791. <https://www.researchgate.net/publication/224771692>.
- ASCE/SEI 41-17 (2017), *Seismic Rehabilitation of Existing Buildings*, American Society of Civil Engineer, New York, U.S.A.
- Asteris, P.G., Kakaletsis, D.J., Chrysostomou, C.Z. and Smyrou, E.E. (2011b), "Failure modes of in-filled frames", *Electronic J. Struct. Eng.*, **11**(1), 11-20. [https://www.researchgate.net/publication/233961174\\_Failure\\_Modes\\_of\\_In-filled\\_Frames](https://www.researchgate.net/publication/233961174_Failure_Modes_of_In-filled_Frames).
- ASTM C1531 (2016), *Standard Test Methods for In-situ Measurement of Masonry Mortar Joint Shear Strength Index*, American Society for Testing and Materials.
- Balik, F.S., Korkmaz, H.H., Kamanli, M., Bahadir, F., Korkmaz, S.Z. and Unal, A. (2013), "An experimental study on reinforced concrete infilled frames with openings", *Advan. Mater. Res.*, **747**, 429-432. <https://doi.org/10.4028/www.scientific.net/AMR.747.429>.
- Bergami, A.V. and Nuti, C. (2015), "Experimental tests and global modeling of masonry infilled frames", *Earthq. Struct.*, **9**(2), 281-303. <https://doi.org/10.12989/eas.2015.9.2.281>.
- Chung, L.L., Wu, L.Y., Yang, Y.S., Ku, T.Y., Lai, Y.A. and Huang, C.T. (2012), "Verification of simplified pushover analysis of school buildings by in-Situ Tests", NCREE Research Programs and Accomplishments, National Center for Research on Earthquake Engineering, Taipei, Taiwan. <https://www.ncree.narl.org.tw/assets/file/101E4.pdf>.
- Construction and Planning Agency Ministry of the Interior (2011), *Seismic Design Specifications and Commentary of Buildings*, Construction and Planning Agency Ministry of the Interior, Taipei, Taiwan.
- Fenerci, A., Binici, B., Ezzatfar, P. and Ozcebe, G. (2016), "The effect of infill walls on the seismic behavior of boundary columns in RC frames", *Earthq. Struct.*, **10**(3), 539-562. <https://doi.org/10.12989/eas.2016.10.3.539>.
- Fiorato, A.E., Sozen, M.A., and Gamble, W.L. (1970), "An investigation of the interaction of reinforced concrete frames with masonry filler walls", Research Report No. UILU-ENG 70-100, Department of Civil Engineering, University of Illinois at Urbana-Champaign, Champaign, I.L., U.S.A. <http://hdl.handle.net/2142/14303>.
- Jiang, W.C., Chiou, T.C., Hsiao, F.P., Tu, Y.S., Chien, W.Y., Yeh, Y.K., Chung, L.L. and Hwang, S.J. (2008), "In-situ static pushover tests of school building at youlin kou-hu school", Research Report No. NCREE-08-044, National Center for Research on Earthquake Engineering, Taipei, Taiwan.
- Kakaletsis, D. and Karayannis, C. (2007), "Experimental investigation of infilled r/c frames with eccentric openings", *J. Earthq. Eng. Mech.*, **26**(3), 231-250. <https://doi.org/10.12989/sem.2007.26.3.231>.
- Kakaletsis, D. and Karayannis, C.G. (2008), "Influence of masonry strength and openings on infilled R/C frames under cycling loading", *J. Earthq. Eng.*, **12**(2), 197-221. <https://doi.org/10.1080/13632460701299138>.
- Lin, B.C. (2011), "Experiment and Analysis of Confined Masonry Wing-walls under In-plane Loading", Master's Thesis, National Cheng Kung Univ., Tainan.
- Lo, T.Y. (2010), "Masonry Infill Panels under In-plane Loading", Master's Thesis, National Cheng Kung Univ., Tainan.
- Lourenço, P.B., Leite, J.M., Paulo-Pereira, M.F., Campos-Costa, A., Candeias, P.X. and Mendes, N. (2016), "Shaking table testing for masonry infill walls: unreinforced versus reinforced solutions: Shaking table testing for masonry infill walls", *Earth Eng Struct. Dyn.*, **45**(14), 2241-2260. <https://doi.org/10.1002/eqe.2756>.
- Maidiawati, Tanjung, J., Hayati, Y., Agus and Medriosa, H. (2019), "Experimental investigation of seismic performance of reinforced brick masonry infilled reinforced concrete frames with a central opening", *Int. J. Geomate.*, **16**(57), 35- 41. <https://doi.org/10.21660/2019.57.4592>.
- Mansouri, A., Marefat, M.S. and Khanmohammadi, M. (2013), "Experimental evaluation of seismic performance of low-shear strength masonry infills with openings in reinforced concrete frames with deficient seismic details", *Struct Des Tall Spec.*, **23**(15), 1190-1210. <https://doi.org/10.1002/tal.1115>.
- Mosalam, K.M., White, R.N. and Gergely, P. (1997), "Static response of infilled frames using quasi-static experimentation", *J. Struct. Eng.*, **123**(11), 228-237. [https://doi.org/10.1061/\(ASCE\)07339445\(1997\)123:11\(1462\)](https://doi.org/10.1061/(ASCE)07339445(1997)123:11(1462)).
- Okail, H., Abdelrahman, A., Abdelkhalik, A. and Metwaly, M., (2016), "Experimental and analytical investigation of the lateral load response of confined masonry walls", *J Hbrc.*, **12**(1), 33-46. <http://dx.doi.org/10.1016/j.hbrcj.2014.09.004>.
- Ozturkoglu, O., Ucar, T. and Yesilce, Y. (2017), "Effect of masonry infill walls with openings on nonlinear response of reinforced concrete frames", *Earthq. Struct.*, **12**(3), 333-347. <https://doi.org/10.12989/eas.2017.12.3.333>.
- Penava, D., Anić, F., Sarhosis, V. and Abrahamczyk, L. (2019), "Distribution of shear resistance among components Of R.C. frames with masonry infill walls containing confined door and window openings", *Proceedings of the 7th International Conference on Computational Methods in Structural Dynamics and Earthquake Engineering*, June.
- Shah, S.A.A., Khan, J.S., Ali, S.M., Shahzada, K., Ahmad, W. and Shah, J. (2019), "Shake table response of unreinforced masonry and reinforced concrete elements of special moment resisting frame", *Advan. Civil Eng.* <https://doi.org/10.1155/2019/7670813>.
- Sigmund, V. and Penava, D. (2012), "Experimental study of masonry infilled R/C frames with opening", *Proceedings of the 15th World Conference on Earthquake Engineering*, Lisbon, Portugal, September.
- Stavridis, A. (2009), "Analytical and experimental study of seismic performance of reinforced concrete frames infilled with masonry walls", Ph.D. Dissertation, University of California,

- San Diego, U.S.A.
- Stavridis, A., Koutromanos, I. and Shing, P. (2012), "Shake-table tests of a three-story reinforced concrete frame with masonry infill walls", *Earth Eng. Struct. Dyn.*, **41**(6), 1089-1108.
- Stavridis, A., Tempestti, J.M. and Bose, S. (2017), "Updating the ASCE 41 Provisions for Infilled RC Frames", *Proceedings of 2017 SEAOC Convention*, San Diego, U.S.A, September.
- Tekeli, H. and Aydin A. (2017), "An experimental study of the seismic behavior of Infilled RC frames with opening", *Scientia Iranica.*, **24**(5), 2271-2282.  
<https://doi.org/10.24200/sci.2017.4150>.
- Tu, Y.H., Chuang, T.H., Lin, P.C., Weng, P.W. and Weng, Y.T. (2011), "Experiment of slender confined masonry panels under monotonic and cyclic loading", *Proceedings of the 15th World Conference on Earthquake Engineering*, Lisbon, Portugal, September.
- Tu, Y.H., Lo, T.Y. and Chuang, Y.T. (2020), "Lateral loading test for partially confined and unconfined masonry panels", *Earthq. Struct.*, **18**(3), 379-390.  
<https://doi.org/10.12989/eas.2020.18.3.379>.
- Tu, Y.H., Yeh, P.L., Liu, T.W. and Jean, W.Y. (2009), "Seismic Damage evaluation for low-rise RC school buildings in Taiwan", *Proceedings of the 2009 Structures Congress*, Austin, Texas, U.S.A, April.
- Voon, K.C. and Ingham, J.M. (2008), "Experimental in-Plane Strength investigation of reinforced concrete masonry walls with openings", *J. Struct. Eng.*, **134**(5), 758-768.  
[https://doi.org/10.1061/\(ASCE\)07339445\(2008\)134:5\(758\)](https://doi.org/10.1061/(ASCE)07339445(2008)134:5(758)).
- Wang, Lei., Qian, K., Fu, F. and Deng, X.F. (2019), "Experimental study on the seismic behaviour of reinforced concrete frames with different infill masonry", *Magazine Concrete Res.*,  
<https://doi.org/10.1680/jmacr.18.00484>.
- Weng, Y.T., Lin, K.C., Hwang, S.J. and Chiou, T.C. (2008), "In-situ pseudo- dynamic tests and cyclic pushover test of existing school building", Research Report No. NCREE-08-004, National Center for Research on Earthquake Engineering, Taipei, Taiwan